Colloid and Polymer Science (2018) 296:653–667
https://doi.org/10.1007/s00396-018-4277-z

ORIGINAL CONTRIBUTION

Preparation and characterization of poly(acrylic acid-co-acrylamide) /montmorillonite composite and its application for methylene blue adsorption

Congcong Wei[1,2] · Zhiqun Xu[1,2] · Fuhao Han[1,2] · Wenkai Xu[1,2] · Junjie Gu[1,2] · Minrui Ou[1,2] · Xiaoping Xu[1,2]

Received: 28 October 2017 / Revised: 6 January 2018 / Accepted: 19 January 2018 / Published online: 21 February 2018

Abstract

A series of poly(acrylic acid-co-acrylamide)/montmorillonite composite (poly(AA-co-AM)/MMT) was prepared by radical polymerization. The composite was characterized by Fourier transform infrared spectroscopy (FTIR), scanning electron microscope (SEM), energy dispersive X-ray (EDX) and X-ray diffraction (XRD). Batch adsorption experiments of methylene blue (MB) from aqueous solutions were carried out with poly(AA-co-AM)/MMT composite. The effects of montmorillonite (MMT) content, initial pH of MB solutions, adsorption temperature, and ionic strength on the adsorption were investigated. Furthermore, the adsorption kinetics and isotherms were studied by analyzing the effect of adsorption time and initial MB concentration on the adsorption capacity. The results indicated that the addition of a small amount of MMT could improve the adsorption capacity of the poly(AA-co-AM). The maximum adsorption capacity of poly (AA-co-AM)/MMT (2%) composite was 1964.1 mg g^{-1}. The adsorption kinetics were in good agreement with the pseudo-second-order equation, and the adsorption isotherms were better fitted for the Langmuir equation. In addition, desorption studies show that the composites have good regenerative properties. The experimental results show that the poly(AA-co-AM)/MMT can be used as promising adsorbent for the removal of MB from wastewater.

Keywords Composites · Hydrogels · Montmorillonite · Adsorption · Methylene blue

Introduction

Synthetic dyes were widely used in textile, paper, leather, food, cosmetics, plastics, and other fields [1]. A large amount of untreated dye wastewater was discharged directly into natural water bodies every year. Dye wastewater was characterized by high organic content, high chromaticity, complex composition, and poor biodegradability, so it was widely recognized as one of the intractable industrial wastewaters [2]. Even if a small amount of dye wastewater was discharged into the water, it also can greatly reduce the light transmittance of water bodies and hinder the photosynthesis of aquatic plants [3]. In addition, some dyes or their metabolites are biologically toxic, even carcinogenic and mutagenic, which poses a huge threat to human health [4]. For example, methylene blue (MB) is a widely used cationic dye, which can cause eye burns. And through oral intake, it will produce burning sensation, causing nausea, vomiting, sweating, mental disorders, or methemoglobinemia [5]. Therefore, the effective treatment of dye wastewater is still an important field of widespread concern.

There are many methods to remove dyes from wastewater, such as membrane separation [6], coagulation and flocculation [7], electrocatalysis [8], oxidation or ozonation [9], biodegradation [10], and adsorption. Among these methods, the adsorption method, with its low cost, high speed, and large capacity and that its adsorbent can be recycled and other advantages, becomes the most effective and commonly used wastewater decolorization method [11]. At present, activated carbon is the most widely used commercial adsorbent. However, the market price of industrial-grade activated carbon is considered

✉ Xiaoping Xu
xu@fzu.edu.cn

[1] Key Laboratory of Pharmaceutical preparations, College of Chemistry, Fuzhou University, Fuzhou 350108, People's Republic of China

[2] Key Laboratory of Bipharmaceutical, College of Chemistry, Fuzhou University, Fuzhou 350108, People's Republic of China

very expensive (average cost about US$7.5/kg) [12]. In addition, activated carbon has some disadvantages such as low adsorption capacity, complicated and expensive regeneration process, large loss of adsorbent, and no selectivity and ineffectiveness for disperse dyes and vat dyes [13]. These shortcomings have greatly restricted the practical value of activated carbon and prompted many researchers to find more economical adsorbents.

Hydrogel is a kind of polymer material with three-dimensional network structure, which is composed of hydrophilic homopolymer or copolymer [14]. It can swell in aqueous solution; has good water permeability, biocompatibility, and biodegradability; and can perceive and respond to environmental changes [15]. Hydrogel contains a large number of functional groups, such as hydroxyl, amino, carboxyl, and amide groups, which have strong binding capacity for cationic dyes. However, these polymers have some limitations such as poor mechanical properties, poor thermal stability, and low porosity [16]. Due to its low cost, abundant distribution, and high adsorption properties, natural clay minerals can be used as wastewater treatment adsorbents. According to different layered structures, clay minerals are mainly divided into montmorillonite, mica, kaolinite, apatite, vermiculite, and sepiolite [17]. Among them, montmorillonite clay has the largest surface area and cation exchange capacity, and the current market price (about US$0.04–0.12/kg) is much lower than of activated carbon [13]. The excellent adsorption property and low price of montmorillonite clay have attracted the attention of many researchers [18–20]. However, in practical applications, clay adsorbent still has the disadvantages of poor dispersibility, difficulty in solid-liquid separation, and poor reusability [21].

In recent years, researchers have prepared a series of polymer/clay composites by doping clay minerals in polymer systems. Marrakchi, F [22] reported a cross-linked chitosan/sepiolite composite for the adsorption of methylene blue and reactive orange 16 dyes. Shirsath, SR [23] synthesized poly (acrylamide)-kaolin composite hydrogel by ultrasonic-assisted in situ emulsion polymerization to remove crystal violet dye from wastewater. Ayazi, Z [24] synthesized alginate-montmorillonite-polyaniline nanocomposite and optimized the reactive orange 13 adsorption conditions by the response surface methodology. Polymer/clay mineral composite combines the advantages of both, maintaining high adsorption capacity while dramatically reducing costs and improving material properties (mechanical strength, thermal stability, material porosity, and reusability).

In this paper, we report a novel composite of poly(AA-co-AM)/montmorillonite (MMT), which is used as an adsorbent for the removal of cationic dye MB (molecular structure is shown in Scheme 1a) in aqueous solutions. The composites were characterized by Fourier transform infrared spectroscopy (FTIR), scanning electron microscope (SEM), energy dispersive X-ray (EDX), and X-ray diffraction (XRD). The effects of MMT content, pH value, interference ionic strength, and adsorption temperature were studied. In addition, the adsorption kinetics and adsorption isotherm parameters were also evaluated in detail. Finally, the desorption and reusability of the composites were also investigated. The experimental results show that the poly(AA-co-AM)/MMT composite can be used as promising adsorbent for the removal of cationic dye from wastewater.

Materials and method

Materials

Acrylic acid (AA), acrylamide (AM), methylene blue (MB), *N*,*N*,-methylenebisacrylamide (MBA), sodium nitrate ($NaNO_3$), and magnesium nitrate hexahydrate ($Mg(NO_3)_2 \cdot 6H_2O$) and iron(III) nitrate nonahydrate ($Fe(NO_3)_3 \cdot 9H_2O$) were all obtained from Sinopharm Chemical Reagent Co., Ltd. Sodium hydrogen sulfite (SHS), sodium hydroxide (NaOH), and hydrochloric acid were all purchased from Xilong Chemical Co., Ltd. Ammonium persulfate (APS) was supplied by Shanghai SANGON Biological Engineering Co., Ltd. Sodium montmorillonite (Na-MMT) was supplied by Nanocor Inc., USA. The cationic exchange capacity (CEC) of MMT-Na is 145 mequiv/100 g, with a purity greater than 98%, with a methylene blue adsorption capacity of 437.7 mg L^{-1} and with 16–22 μm particle size. The chemical compositions of MMT-Na are given in Table 1. All chemicals were of analytical grade and used without further purification. All aqueous solutions were prepared with deionized water.

Preparation of poly(AA-co-AM)/MMT composite adsorbent

In this paper, a series of poly(AA-co-AM)/MMT composite was prepared by radical polymerization. The specific preparation method was as follows. First, 8 g of AA and 20 mL of distilled water were placed in a 100-mL beaker with mechanical stirring at room temperature. Then, 3.55 g of NaOH was dissolved in 10 mL of distilled water and added drop-wise to the mixture in an ice bath so that AA was partially neutralized to 80%. Then, 2 g of AM and different amounts of MMT were added and stirred for 30 min. Then, 0.08 g of MBA was dissolved in 5 mL of distilled water, added to the mixture, and stirred for 15 min. Finally, 0.06 g of APS and 0.06 g of SHS were dissolved in 5 mL of distilled water and added to the mixture to initiate the polymerization reaction. The mixture was reacted in a water bath at 50 °C for 1 h and then reacted at 70 °C for 2 h. After completion of the polymerization reaction, the sample was chopped and rinsed with deionized water until

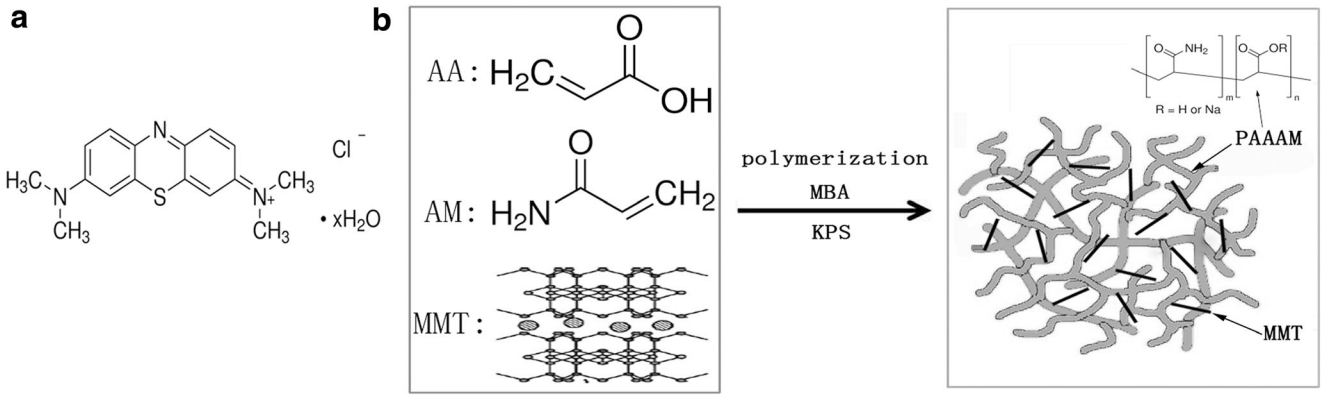

Scheme 1 **a** Structure of MB. **b** Synthesis process of poly(AA-co-AM)/MMT composite

the unreacted material was completely removed and dried in a vacuum freeze drier for 24 h to constant weight. The product was then milled and passed through a 100-mesh screen and used for further experiments. Synthesis process of composite material is as shown in Scheme 1b.

Characterization methods

FTIR spectra of the samples were recorded by a Fourier transform infrared spectrometer (Nicolet Magna 670) in the range of 4000–400 cm^{-1}. The morphology and composition of the samples were measured by field-emission scanning electron microscopy (FE-SEM, Nova NanoSEM 230, FEI, USA) and energy dispersive X-ray (EDX) spectrometer. The crystal structures of the samples were characterized by an X-ray diffractometer (XRD, Empyrean, PANalytical, Netherlands) with Cu Kα radiation. The MB concentrations in aqueous solutions were determined using a UV-Vis spectrophotometer (UV-1780, Shimadzu, Japan) at 665 nm according to the calibration curve.

Adsorption experiments

All batch adsorption experiments were carried out in 20 mL of MB aqueous solution with 20 mg of the adsorbent and shaking at 150 rpm on a thermostatic shaker. After a certain period of time, the sample was taken from the shaker and the mixture was centrifuged by a high-speed centrifuge. The absorbance of MB in the supernatant was measured at 665 nm using a UV-Vis spectrophotometer, and the MB concentration remaining in the solution was calculated by the calibration curve. Finally, the adsorption capacity and adsorption efficiency of adsorbent to MB was calculated according to the following formula:

$$q_e = \frac{(C_0 - C_e)\,V}{m} \quad (1)$$

$$\%\text{adsorption} = \frac{C_0 - C_e}{C_0} \quad (2)$$

where q_e is the equilibrium adsorption capacity of adsorbent (mg g^{-1}); C_0 and C_e are the initial and equilibrium concentration of the MB solution, respectively (mg L^{-1}); m is the weight of the adsorbent (mg), and V is the volume of the MB solution (mL).

The effect of MMT content on MB removal was studied by adding adsorbents with different MMT contents to MB solution (2000 mg L^{-1}, pH 5.0) and adsorbing at 25 °C for 120 min. The MB solution (2000 mg L^{-1}) was adjusted to different pH by using a pH meter and adsorbed at 25 °C for 120 min to study the effect of pH on MB removal. The effect of temperature on MB removal was investigated by adjusting the thermostatic shaker to different temperature and adsorbing MB solution (2000 mg L^{-1}, pH 5.0) for 120 min. The effect of ionic strength on MB removal was investigated by adding different concentrations of interfering ions to the MB solution (2000 mg L^{-1}, pH 5.0) and adsorbing at 25 °C for 120 min. In addition, the adsorption kinetics were studied by adding 20 mg of adsorbent to 20 mL of MB solution (2000 mg L^{-1}, pH 5.0) and shaking at 25 °C for predetermined time interval. The adsorption isotherms was investigated by adding 20 mg of adsorbent to 20 mL of different concentrations of MB solution (pH 5.0) and adsorbing at 25 °C for 120 min. Each experiment was run in triplicate and the average data were presented.

Table 1 The chemical composition of sodium montmorillonite (wt%)

Composition	SiO_2	Al_2O_3	Na_2O	MgO	Fe_2O_3	CaO	K_2O	Ti_2O
Proportion	61.932	23.278	6.415	3.913	3.217	0.294	0.217	0.184

Desorption and reusability studies

The desorption performance of the adsorbent for MB was evaluated by the following method. First, 20 mg of the adsorbent was added to 20 mL of MB solution (2000 mg L^{-1}, pH 5.0) and shaken at 25 °C for 120 min. The adsorbent is then recovered with a high-speed centrifuge and washed thoroughly with distilled water to remove unadsorbed dyes. Distilled water (20 mL) of different pH was used as the eluent, and then the loaded adsorbent was placed in different pH eluate and shaken at 25 °C for 60 min. Finally, the MB concentration in supernatant and eluate was measured by UV-Vis spectrophotometer, respectively, and the desorption rate was calculated by the following formula:

$$\%\text{desorption} = \frac{C_d}{C_0 - C_e} \quad (3)$$

where C_0 and C_e are the initial and equilibrium concentration of the MB solution in the adsorption experiment, respectively (mg L^{-1}), and C_d is the equilibrium concentration of MB in the eluent.

The reusability of the adsorbent was studied by five cycles of continuous adsorption-desorption. First, the adsorption experiment was carried out in the same manner as the desorption experiment, and then 20 mg of the loaded adsorbent was desorbed in HCl solution (20 mL, 0.1 M) for 60 min. The sample was then placed in NaOH solution (20 mL, 0.1 M) and shaken at 25 °C for 20 min to neutralize the residual hydrochloric acid. Finally, the adsorbent is sufficiently washed with distilled water for a new adsorption-desorption cycle. Each experiment was run in triplicate and the average data were presented.

Results and discussion

FTIR characterization

The infrared spectra of MMT, poly(AA-co-AM), poly(AA-co-AM)/MMT30%, MB, and poly(AA-co-AM)/MMT30%/MB are shown in Fig. 1. For the MMT (Fig. 1a), 3618 and 912 cm^{-1} respectively correspond to the Al–O–H stretching and bending vibration of the montmorillonite sheet surface, 3424 and 1636 cm^{-1} respectively correspond to the H–O–H stretching and bending vibration of the water molecules in the montmorillonite layer, 1012 cm^{-1} due to Si–O–Si stretching vibration, 797 cm^{-1} is attributed to the α-quartz in montmorillonite, and 512 cm^{-1} due to Si–O–M coupling vibration [25].

For the poly(AA-co-AM) (Fig. 1b), 3346 cm^{-1} corresponds to N–H stretching vibration of AM, 2944 cm^{-1} corresponds to C–H stretching vibration, 1663 cm^{-1} corresponds to C=O bending vibration of AA, 1450 cm^{-1} due to the C–N stretching vibration of AM, and 1550 and 1403 cm^{-1} are attributed to the asymmetric and symmetrical stretching vibration of $–COO^-$, respectively [26]. In addition, C=C stretching vibration in AA and AM did not appear, indicating that copolymerization of AA and AM monomers occurred.

For the poly(AA-co-AM)/MMT30%(Fig. 1c), 3350 cm^{-1} is attributed to the superposition of the stretching vibrations of O–H and N–H in poly(AA-co-AM); 2941 cm^{-1} corresponds to CH stretching vibration, 1663; and 1550, 1450, and 1403 cm^{-1} correspond to the characteristic peaks of poly(AA-co-AM). Compared with Fig. 1b, c, the new peaks at 1031, 513, and 452 cm^{-1} are attributed to Si–O–Si stretching vibration, Si–O–M coupling vibration, and M–O coupling vibration in montmorillonite, respectively. In addition, the Al–O–H stretching vibration (3618 cm^{-1}) due to the MMT surface almost disappears, indicating that montmorillonite is not simply mixed in the polymer matrix, and the Al–O–H on the MMT surface may also be involved in the copolymerization.

The infrared spectra of MB (Fig. 1d) and poly(AA-co-AM)/MMT30%/MB (Fig. 1e) were analyzed comparatively. It can be seen that the new peaks at 1598 and 1489 cm^{-1}(Fig. 1e) belonged to the aromatic ring skeleton stretching vibration of MB. In addition, the new peaks at 1334, 1138, and 885 cm^{-1} correspond to the $–CH_3$ symmetrical bending vibration, C–S stretching vibration, and C–H surface bending vibration of MB, respectively [27], indicating that MB was successfully adsorbed on poly(AA-co-AM)/MMT composites.

XRD characterization

The main diffraction peaks of the MMT minerals in Fig. 2 have been labeled, among which 001, 002, 110, 004, 220, 310, and 330 are the characteristic diffraction peaks of Na-MMT, while 100, 101, and 112 are the characteristic diffraction peaks of detrital minerals (α-quartz) in MMT minerals [28]. The strong diffraction peak of MMT at $2\theta = 7.12°$ is the reflection from the (001) basal plane [29], and the corresponding interlayer spacing $d001 = 1.241$ nm is calculated by the Bragg equation ($2d\sin\theta = n\lambda$). In addition, poly(AA-co-AM) is completely amorphous with no diffraction peaks. The characteristic diffraction peaks of MMT in poly(AA-co-AM)/MMT30% composites still exist, which proves that MMT was effectively incorporated into poly(AA-co-AM) matrix. And the d001 value is almost unchanged, indicating that the monomers are mainly polymerized between the montmorillonite particles. In addition, the characteristic diffraction peaks of MMT in poly(AA-co-AM)/MMT2% composites are hardly observed. This may be due to the relatively low content of montmorillonite in the composite.

Structural and morphology characterization

The SEM images of poly(AA-co-AM) and poly(AA-co-AM)/MMT30% (before and after adsorption) are shown in Fig. 3. SEM analysis showed that the surface of poly(AA-co-AM)

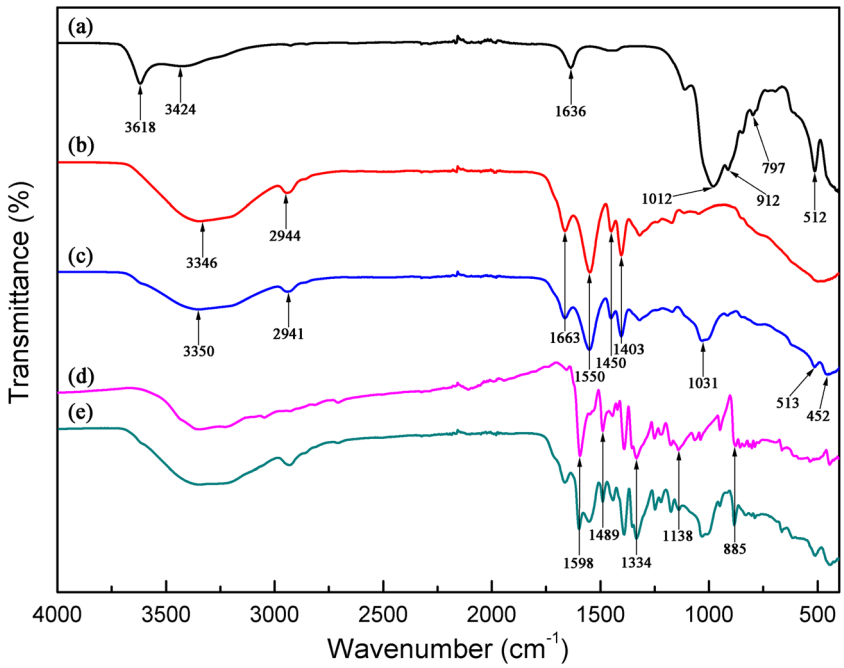

Fig. 1 FTIR spectra of **a** MMT, **b** poly(AA-co-AM), **c** poly(AA-co-AM)/MMT30%, **d** MB, and **e** poly(AA-co-AM)/MMT30%/MB

was dense and smooth, and the introduction of MMT made the composite surface rough and porous. This facilitates dye penetration and adsorption onto the polymer network, thereby increasing adsorption capacity. In addition, comparing the SEM images of poly(AA-co-AM)/MMT30% before and after adsorption, it was found that the irregular sheet structure on the surface of the adsorbent disappeared and covered with many particles.

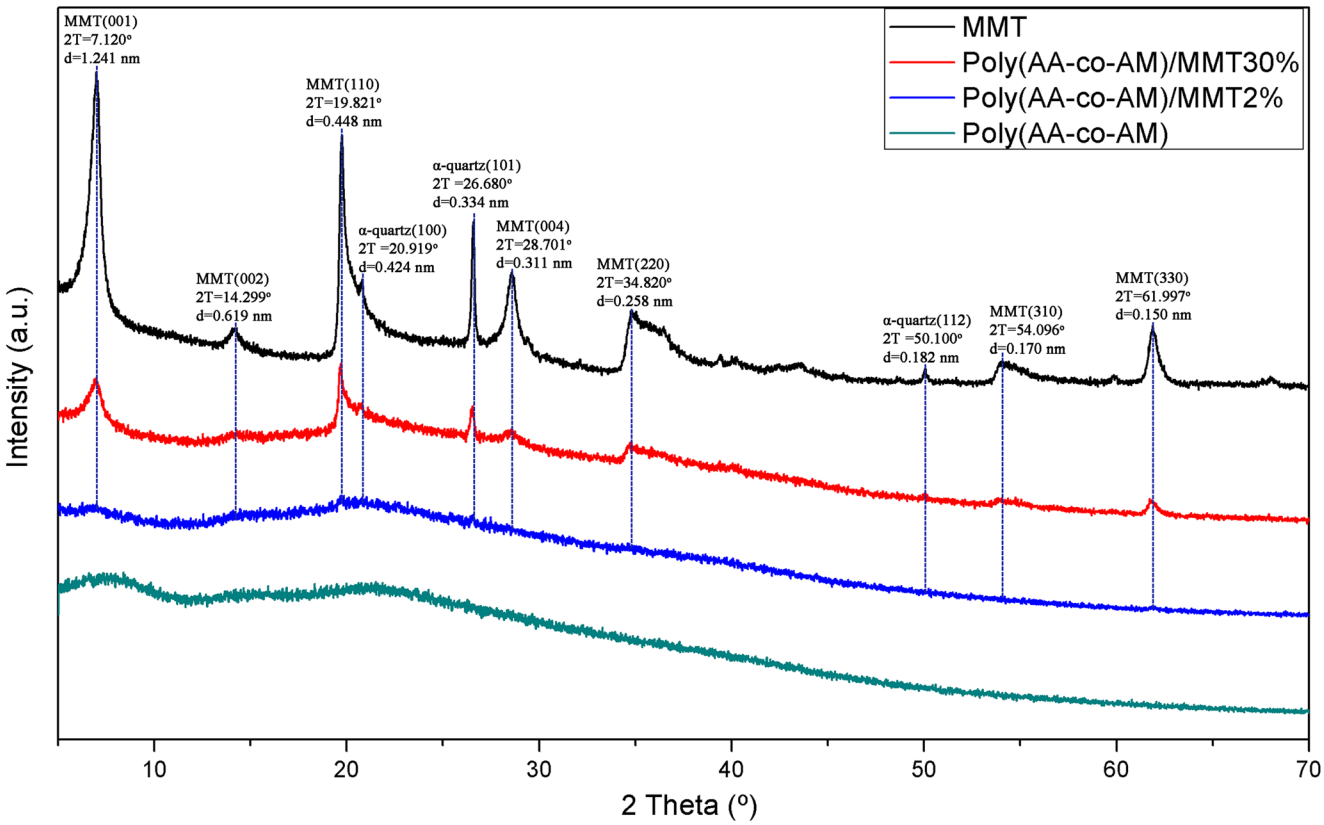

Fig. 2 XRD patterns of MMT, poly(AA-co-AM)/MMT, poly(AA-co-AM)/MMT2%, and poly(AA-co-AM)/MMT30%

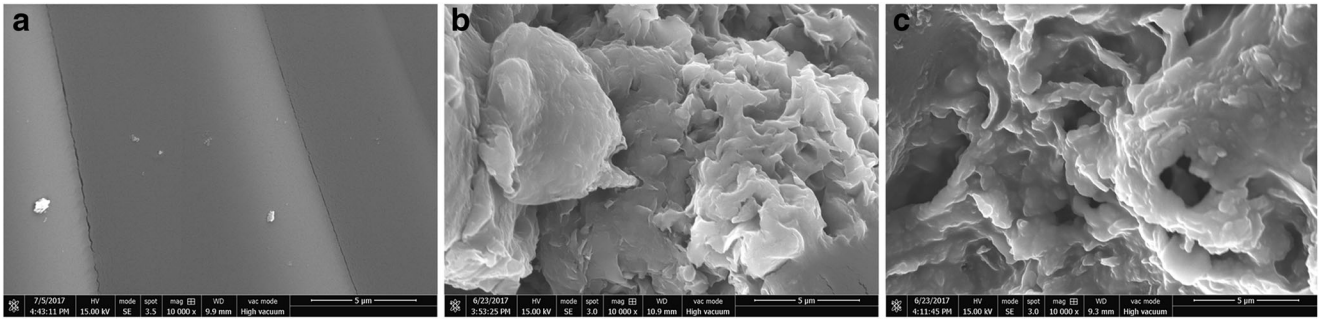

Fig. 3 SEM images of **a** poly(AA-co-AM), **b** poly(AA-co-AM)/MMT30%, and **c** poly(AA-co-AM)/MMT30%/MB

The EDX spectra of poly(AA-co-AM) and poly(AA-co-AM)/MMT30% (before and after adsorption) are shown in Fig. 4. EDX analysis showed that the poly(AA-co-AM)/MMT contains characteristic elements (Mg, Al, Si) of montmorillonite, indicating that the poly(AA-co-AM)/MMT composite has been successfully prepared. The characteristic element (S) of MB appeared on the EDX spectra of poly(AA-co-AM)/MMT (after adsorption), indicating that MB was successfully adsorbed onto poly(AA-co-AM)/MMT. In addition, comparing the EDX spectra of poly(AA-co-AM)/MMT (before and after adsorption), it was found that the content of Na decreases while the content of S increases. This may be that the MB cationic dye replaced the Na ion in the –COONa group by ion exchange. Alternatively, –COONa was ionized in an alkaline environment to produce –COO–, which adsorbs the MB cationic dye by electrostatic attraction.

Effect of MMT content (wt%) on adsorption

The introduction of inorganic clay components can reduce the cost of materials, and the clay content has an important effect on the performance of the polymer system [30]. The influence of MMT content on the adsorption of poly(AA-co-AM)/MMT composite is shown in Fig. 5. The adsorption capacity of the polymer system was increased from 1878 to 1935 mg g^{-1} after the introduction of 2% MMT. According to the FTIR analysis of the composites, the –OH of the montmorillonite surface participates in the polymerization reaction and acts as a crosslinking point in the network, which can improve the polymer network structure and adsorption capacity. In addition, according to XRD and SEM analysis, the introduction of MMT made the composite surface rough and porous, which is conducive to dye penetration and adsorption to the polymer network, thereby enhancing the adsorption capacity. However, a further increase in MMT content reduced the adsorption capacity of the composite. The higher MMT content will produce excessive crosslinking point, which leads to higher crosslinking densities and lower elasticity of the polymer chains, thereby reducing the adsorption capacity of composites [31]. Furthermore, pure MMT has a lower MB adsorption capacity(437.7 mg L^{-1}) and a higher MMT content reduces the content of –COO– groups in the polymer composite, which is also an important reason for the decrease of adsorption capacity [32]. Therefore, we selected blank samples, the best samples (containing 2% MMT), and the cheapest samples (including 30% MMT) for further experiments.

Effect of pH value on adsorption

The pH of dye solution can affect the degree of ionization of adsorbent and the molecular structure of dye, which is an important factor affecting the removal of dye [33]. The effect of the pH value of the dye solution on the adsorption of poly(AA-co-AM)/MMT is shown in Fig. 6. The adsorption capacity of the adsorbent increased sharply with the increase of the initial pH value. However, when the pH was increased to 5.0, the adsorption amount of MB was almost constant. This is because when the pH is low, the excess H^+ in the solution causes the carboxyl groups in the adsorbent to be mostly in the form of –COOH. At the same time, H^+ also competes with cationic dye MB for the adsorption site of the adsorbent. When the pH value is gradually increased, the –COOH groups in the adsorbent dissociate to form –COO–, increasing the electrostatic attraction of the adsorbent to MB, thus increasing the adsorption capacity of MB. In addition, electrostatic repulsion between adjacent $–COO^-$ groups in the polymer network causes the adsorbent to swell highly in the dye solution, which is also an important reason for the increased adsorption capacity. And the pKa of polyacrylic acid is about 4.7 [34]; the adsorption capacity of MB is almost constant due to the buffering effect between –COOH and –COO– groups when the pH reaches 5.0. Thus, further studies of MB adsorption on poly(AA-co-AM)/MMT were carried out at pH = 5.0.

Effect of temperature on adsorption

The effect of ambient temperature on the adsorption of poly(AA-co-AM)/MMT is shown in Fig. 7. When the temperature rose from 15 to 35 °C, the adsorption capacity of

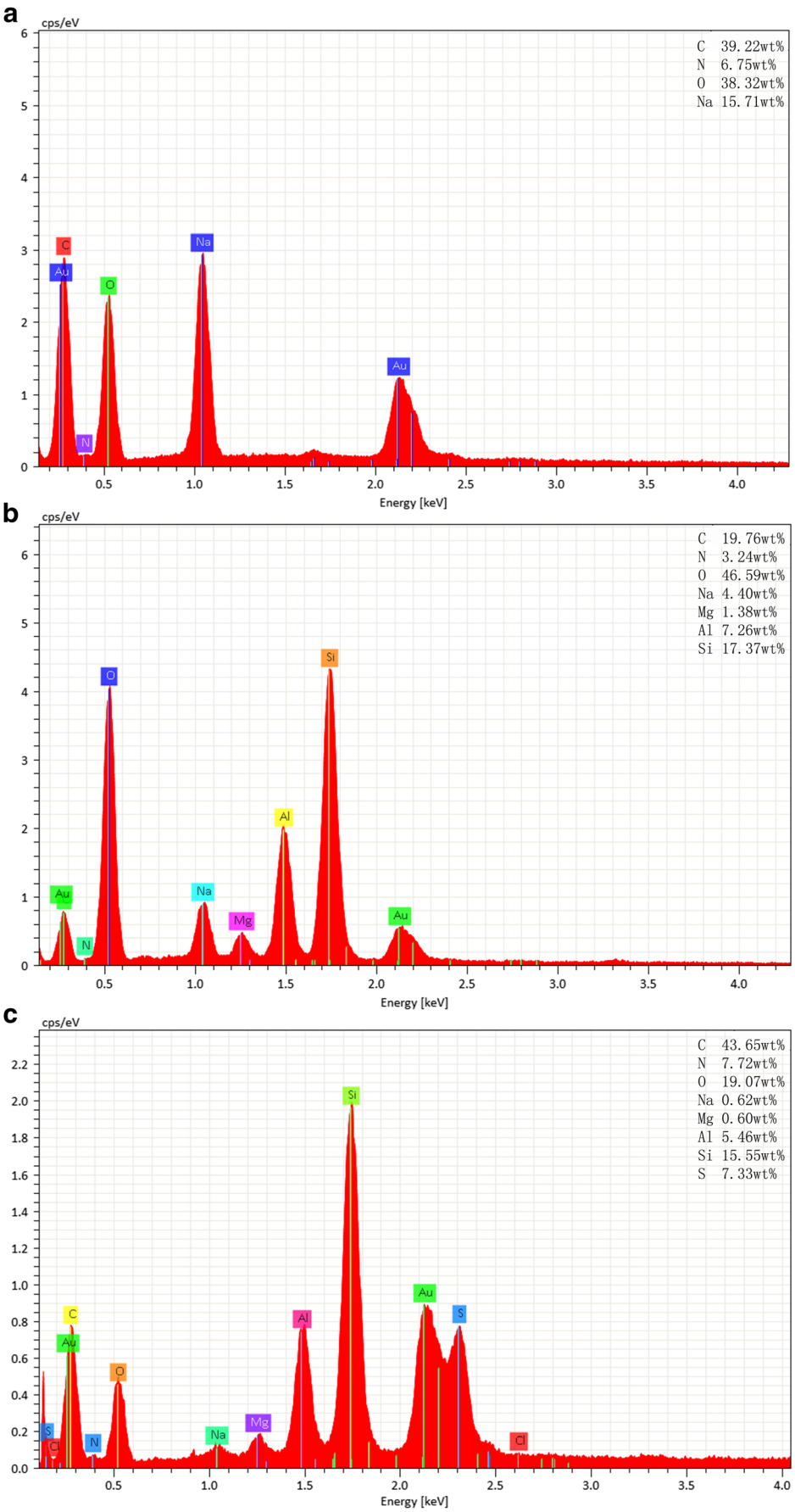

Fig. 4 EDX spectra of **a** poly(AA-co-AM), **b** poly(AA-co-AM)/MMT30%, and **c** poly(AA-co-AM)/MMT30%/MB

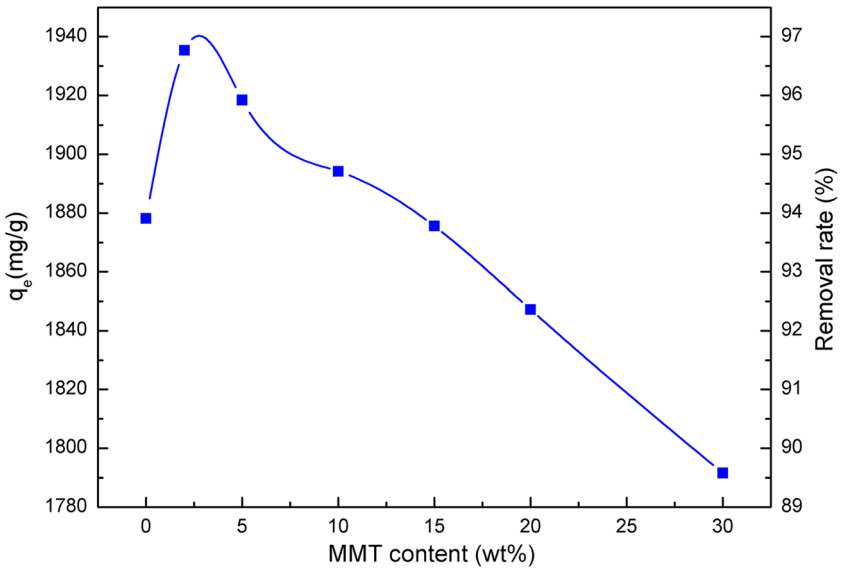

Fig. 5 Effect of MMT content on adsorption of poly(AA-co-AM)/MMT (initial concentrations 2000 mg L^{-1}, adsorption time 2 h, temperature 25 °C and pH value 5.0)

the composites increased. But when the temperature is further increased, the adsorption capacity of the composite material began to decline. The results can be attributed to the following factors. Appropriate elevate temperatures can increase the swelling degree of the adsorbent, which contributes to the diffusion of dye molecules into the interior of the adsorbent. At the same time, increasing the temperature properly can increase the dye diffusion rate and reduce the mass transfer resistance, thus enhancing the adsorption capacity of adsorbent [35]. However, too high temperature destroys the network structure of the polymer and separates the dye molecules that combine with the adsorbent [36]. In addition, since the adsorption process of the MB is exothermic, the high temperature weakens the bond between the adsorbent site and the dye molecule, thereby reducing the adsorption capacity of adsorbent [37].

Effect of ionic strength on adsorption

Figure 8 shows the effect of ionic strength of different cations on the adsorption efficiency of poly(AA-co-AM)/MMT. It was found that as the ionic strength of the cation in the solution increases, the adsorption efficiency of the adsorbent to MB decreases. This is due to the fact that coexisting cations in solution competed with the MB cationic dye for adsorption sites on poly(AA-co-AM)/MMT. In addition, the coexisting cations in the solution may shield the adsorption sites on the adsorbent, weaken the electrostatic attraction between adsorbent and MB, resulting in a decrease in MB removal efficiency. In addition, under the same concentration, the effect of high-valence cations on adsorption efficiency is greater than that of low-valence cations, which may be due to the greater contribution of high-valence cation to ionic strength.

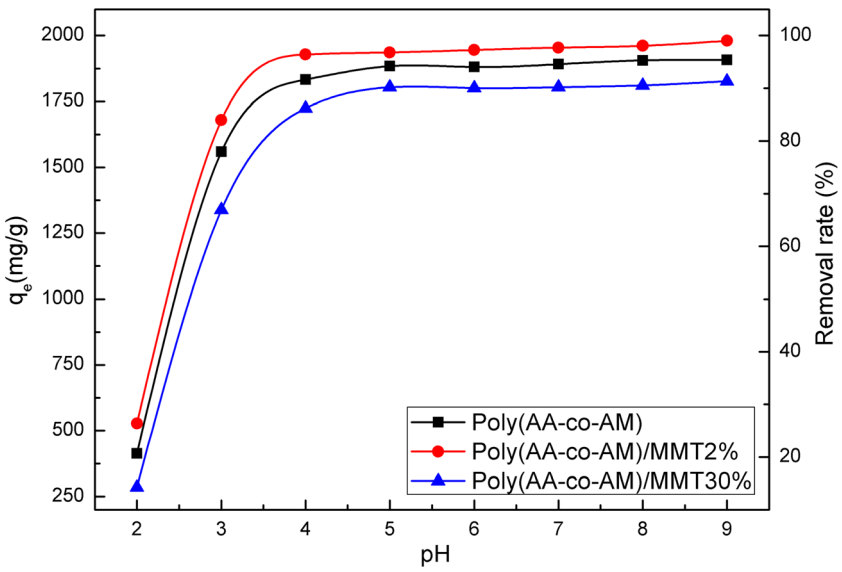

Fig. 6 Effect of the pH on adsorption of poly(AA-co-AM)/MMT (initial concentrations 2000 mg L^{-1}, adsorption time 2 h, and temperature 25 °C)

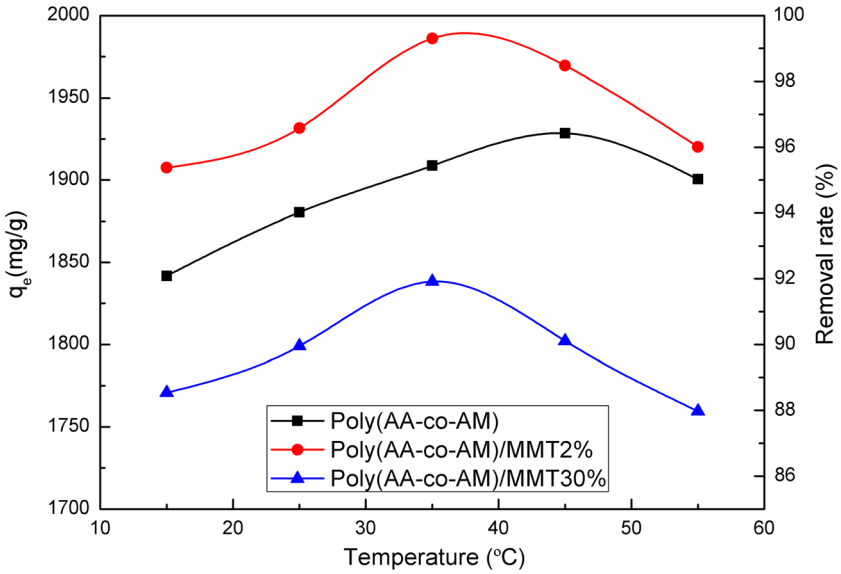

Fig. 7 Effect of the temperature on adsorption of poly(AA-co-AM)/MMT (initial concentrations 2000 mg L^{-1}, adsorption time 2 h, and pH value 5.0)

Adsorption kinetics

The effect of adsorption time on the adsorption of poly(AA-co-AM)/MMT is shown in Fig. 9a. The adsorption amount of MB increased rapidly in the first 15 min, exceeding 90% of the total amount of adsorption. Then, the MB adsorption capacity slowly increased and reached equilibrium after 120 min. In order to study the dynamic interaction between the adsorbate and the adsorbent, the adsorption mechanism was further understood. The adsorption kinetics of MB by poly(AA-co-AM)/MMT was studied by pseudo-first-order kinetics model [38], pseudo-second-order kinetics model [39], and intra-particle diffusion model [40].

The pseudo-first-order kinetics model is expressed as

$$\log(q_e - q_t) = \log q_e - k_1 t \quad (4)$$

The pseudo-second-order kinetics model is expressed as

$$\frac{t}{q_t} = \frac{1}{k_2 q_e^2} + \frac{t}{q_e} \quad (5)$$

The intra-particle diffusion model is expressed as

$$q_t = k_i t^{1/2} + C \quad (6)$$

where t is the adsorption time (min); q_e and q_t are the adsorption capacity (mg g^{-1}) of MB by adsorbent at adsorption equi-

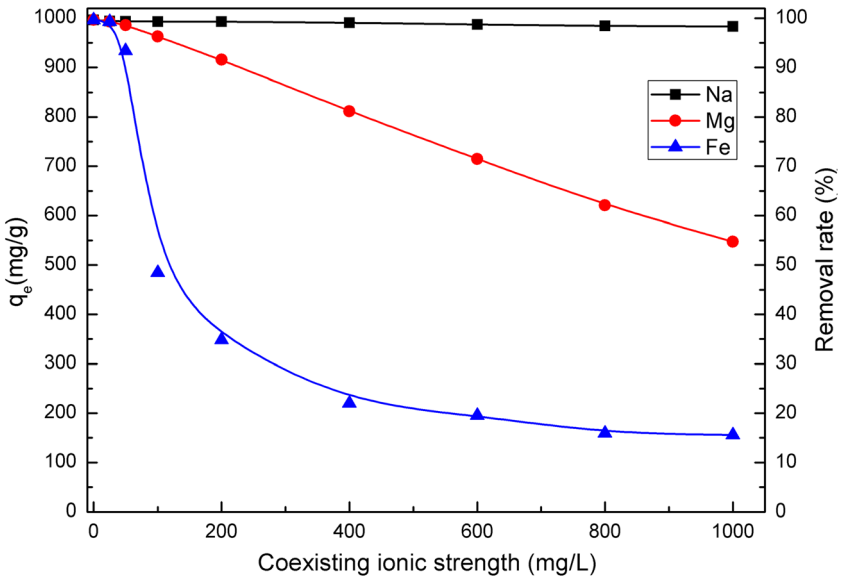

Fig. 8 Effect of the ionic strength on adsorption of poly(AA-co-AM)/MMT (initial concentrations 1000 mg L^{-1}, adsorption time 2 h, temperature 25 °C, pH value 5.0, and MMT content 30%)

librium and time t; k_1 and k_2 are pseudo-first-order rate constants (min^{-1}) and pseudo-second-order rate constants (g mg^{-1} min^{-1}), respectively; k_i is the intra-particle diffusion rate constants (mg g^{-1} $min^{-1/2}$); and C is a constant related to the thickness of the boundary layer.

The obtained kinetic parameters and correlation coefficients are shown in Table 2, and the results of the kinetic fitting curve are shown in Fig. 9. It can be seen from Table 2 that the experimental data are in good agreement with the pseudo-second-order model, and the correlation coefficient (R^2) of the pseudo-second-order model is 0.9999. In addition, the theoretical adsorption capacity($q_{e,cal}$) calculated by the pseudo-second-order kinetic model is very close to the experimental adsorption capacity($q_{e,exp}$). The results show that the adsorption process of MB by poly(AA-co-AM)/MMT follows the pseudo-second-order kinetics model.

As shown in Fig. 9b, the entire adsorption process can be divided into three parts. First is the surface adsorption stage, MB molecules from the solution to the adsorbent surface, the adsorption rate of the fastest. The second stage is the intra-particle diffusion stage, and the MB molecules begin to diffuse into the pores for adsorption. Finally, the adsorption capacity does not change with time, indicating that the adsorption reaction has reached equilibrium [41]. Among them, the intra-particle diffusion stage is the rate control step of the adsorption reaction, where q_t has a good linear relationship with $t_{1/2}$. But the fitting curve does not go through the origin, indicating that the intra-particle diffusion is not the only control step of the adsorption process. The adsorption process may also be affected by the surface adsorption and liquid-film diffusion mechanism [42].

Adsorption isotherms

The effect of MB initial concentration on the adsorption of poly(AA-co-AM)/MMT is shown in Fig. 10. The results showed that when the initial concentration of MB increased from 1600 to 2000 mg L^{-1}, the adsorption capacity of the composites

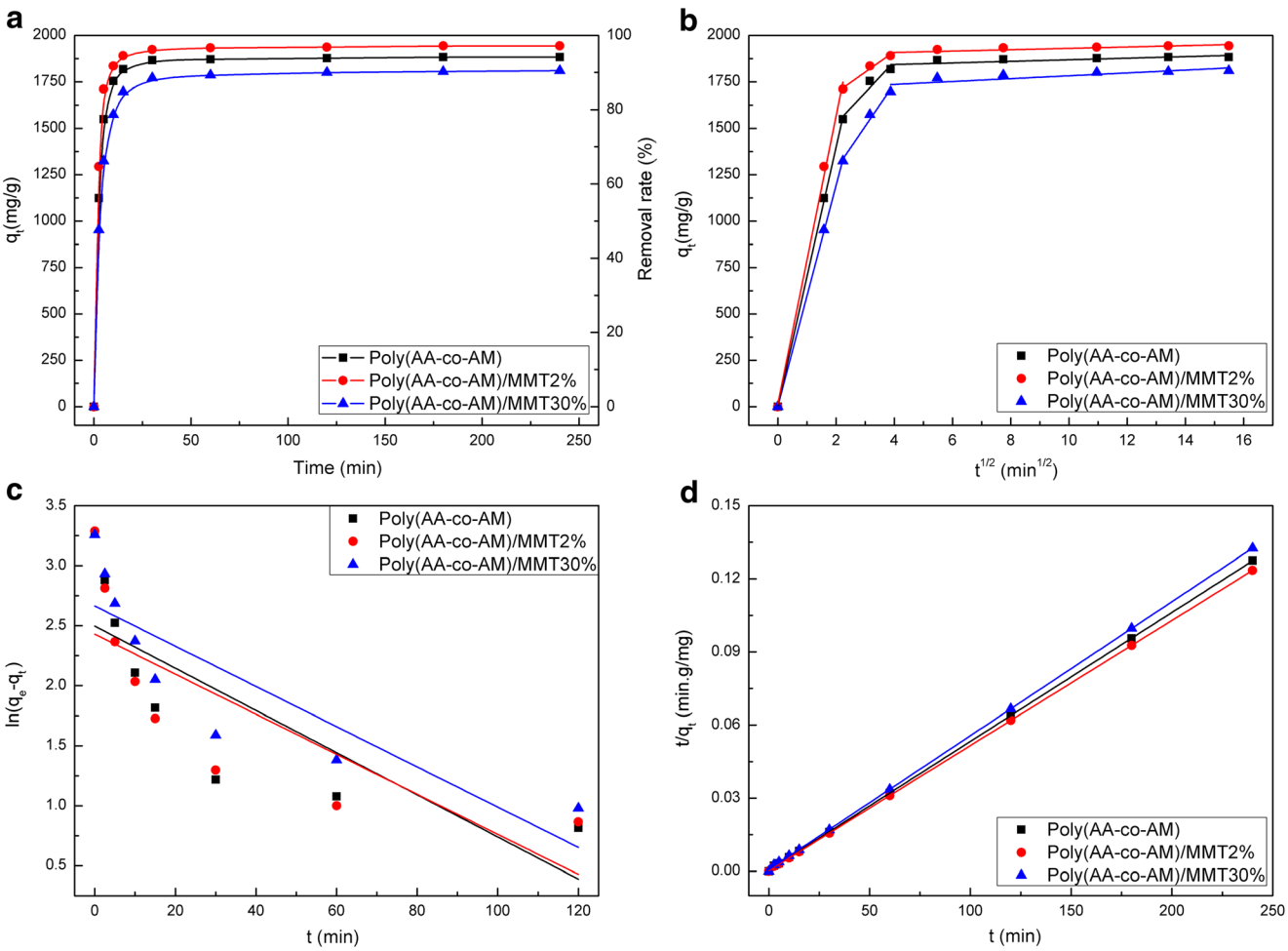

Fig. 9 **a** Effect of the adsorption time on adsorption of poly(AA-co-AM)/MMT, **b** intra-particle diffusion model, **c** pseudo-first-order model, and **d** pseudo-second-order model

Table 2 Kinetic parameters for the adsorption of MB on poly(AA-co-AM)/MMT

MMT(wt%)	$q_{e,exp}$	Pseudo-first-order model			Pseudo-second-order model		
		$q_{e,cal}$	$k_1 \times 10^{-2}$	R^2	$q_{e,cal}$	$k_2 \times 10^{-4}$	R^2
0	1883.2	314.2	1.758	0.6026	1889.9	7.065	0.9999
2	1943.5	269.2	1.669	0.5679	1948.4	8.984	0.9999
20	1809.8	461.9	1.676	0.6823	1819.2	4.365	0.9999

increased rapidly. However, when the initial concentration of MB is further increased, the adsorption capacity of the composite is almost invariable, while the removal rate of MB decreases rapidly. This may be due to that the three-dimensional network space of poly(AA-co-AM)/MMT is substantially filled with MB molecules, so that excess MB molecules are difficult to continue to diffuse into the adsorbent.

The adsorption isotherm can be used to study the interaction between the adsorbent and the adsorbate, thus further explaining the adsorption mechanism [43]. The Langmuir and Freundlich models are two typical adsorption isothermal models. The Langmuir isothermal model assumes that the adsorbate is monolayer adsorbed on the adsorbent surface, and the adsorption sites on the adsorbent surface are evenly distributed, and the adsorbed

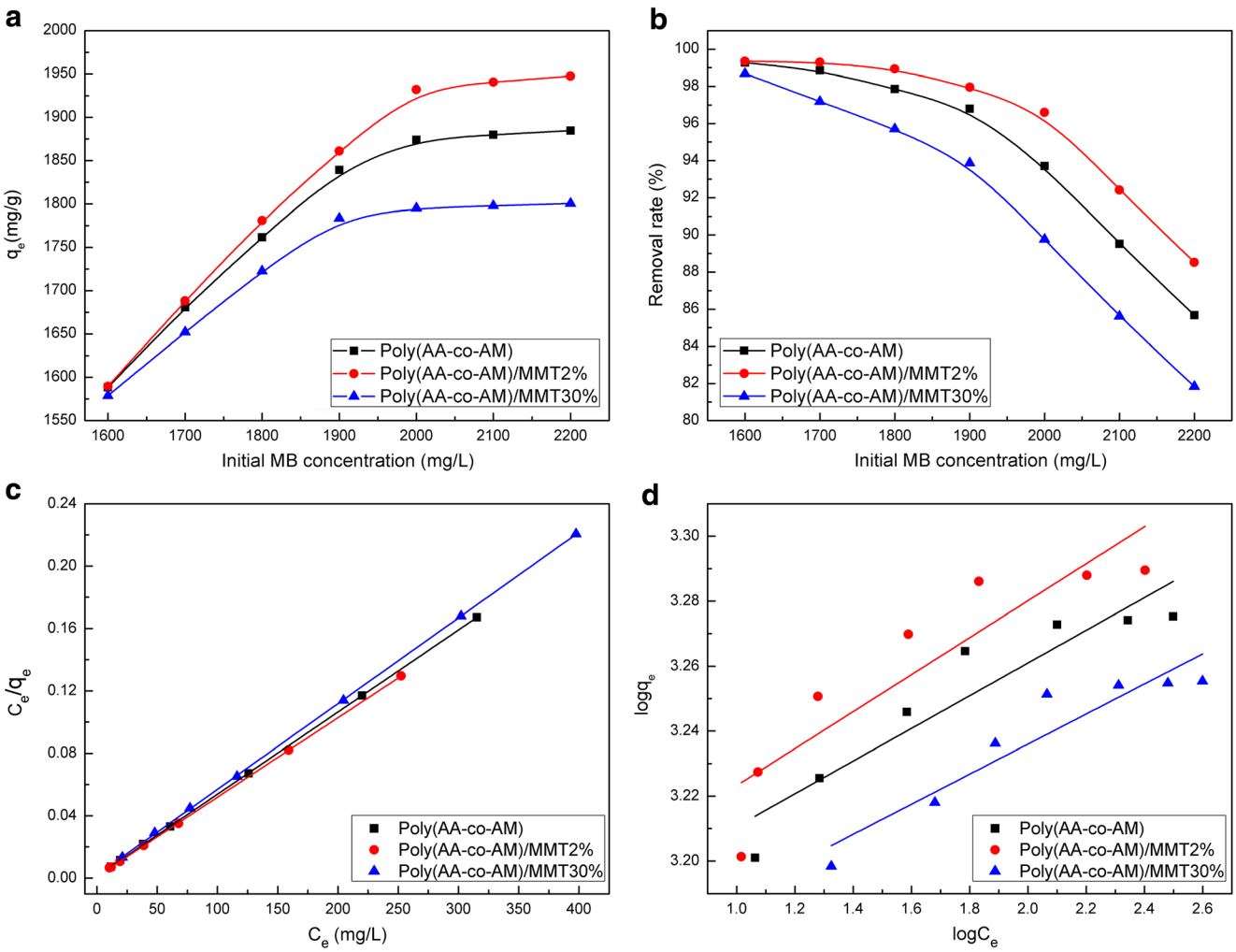

Fig. 10 Effect of the initial MB concentration on adsorption of poly(AA-co-AM)/MMT. **a** Adsorption capacity. **b** Removal rate. Adsorption isotherm plots of MB adsorption onto poly(AA-co-AM)/MMT. **c** Langmuir. **d** Freundlich

Table 3 Isotherm parameters for the adsorption of MB on poly(AA-co-AM)/MMT

MMT (wt%)	$q_{m,exp}$	Langmuir isotherm				Freundlich isotherm		
		$q_{m,cal}$ (mg g^{-1})	K_L (L mg^{-1})	$R_L \times 10^{-3}$	R^2	k_F	1/n	R^2
0	1884.8	1900.3	0.421	1.08–1.48	0.9999	1446.6	0.0503	0.8574
2	1947.6	1964.1	0.512	0.98–1.22	0.9999	1466.73	0.0569	0.7842
20	1800.4	1820.4	0.273	1.66–2.28	0.9999	1391.3	0.0463	0.8689

molecules do not react with each other [44]. R_L is an important dimensionless parameter of the Langmuir isothermal model. The Freundlich model is an empirical adsorption isotherm describing multilayer adsorption and assumes that the adsorption surface is heterogeneous [45]. The equations are represented by the following formulas:

$$\frac{C_e}{q_e} = \frac{1}{bq_m} + \frac{C_e}{q_m} \tag{7}$$

$$\log q_e = \log K_f + \frac{1}{n}\log C_e \tag{8}$$

$$R_L = \frac{1}{1 + bC_0} \tag{9}$$

where C_0 and C_e are the initial and equilibrium concentration of the adsorbate respectively (mg L^{-1}); q_e and q_m are the equilibrium and saturated adsorption capacity of the adsorbent, respectively (mg g^{-1}); b is the Langmuir adsorption equilibrium constant (L mg^{-1}); R_L is the separation factor, which can be used to determine whether it is suitable for adsorption, unfavorable adsorption ($R_L > 1$), linear adsorption($R_L = 1$), favorable adsorption($0 < R_L < 1$), and irreversible adsorption($R_L = 0$) [46]; K_F is the Freundlich adsorption equilibrium constant; and *n* is the constant of adsorption strength, where the smaller the 1/n value, the better the adsorption performance, and the $1/n > 2$ is difficult to adsorb [47].

The adsorption isotherm parameters and correlation coefficients obtained by fitting the experimental data are shown in Table 3, and the results of the isotherm fitting curve are shown in Fig. 10. It can be seen from Table 3 that the experimental data agree well with the Langmuir isothermal model with a correlation coefficient of $R^2 > 0.9999$. And the theoretical maximum adsorption capacity ($q_{m,cal}$) is similar to the experimental adsorption capacity ($q_{m,exp}$). The results showed that the adsorption process of poly(AA-co-AM)/MMT on MB was monolayer. In addition, the separation factor R_L is in the range of 0 to 1, and the Freundlich constant 1/n is much smaller than 2, indicating that the adsorption reaction is prone to occur.

Desorption and reusability studies

Desorption studies can further study the mechanism of adsorption processes. If the distilled water can elute the dye, it can be deduced that the dye molecules are fixed to the adsorbent via the weak bond. If the dye is to be eluted with a strong acid solution, it can be deduced that the dye molecules are immobilized on the adsorbent by ion exchange or electrostatic absorption [48]. Thus, the dye-supported poly(AA-co-AM)/

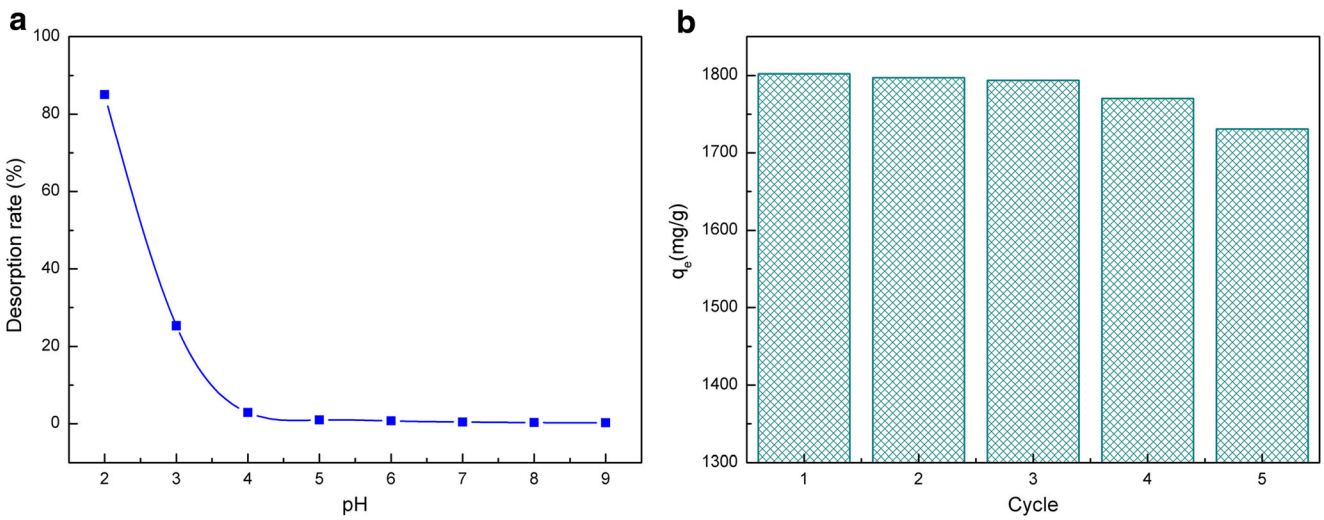

Fig. 11 **a** Effect of pH on desorption percentage of dye from dye-loaded poly(AA-co-AM)/MMT. **b** Reusability of the dye-loaded poly(AA-co-AM)/MMT (initial concentrations 2000 mg L^{-1}, adsorption time 2 h, temperature 25 °C, pH value 5.0, and MMT content 30%)

Table 4 Comparison of adsorption capacity of MB by various adsorbents

Adsorbent	q_{max} (mg g^{-1})	Reference
Fe_3O_4/activated montmorillonite	106.38	[20]
PAA/MGO composites	290.7	[49]
poly(AM-IA)/DAM/$Zr(OH)_4$ composite	102	[50]
HNTs/Fe_3O_4/poly(DA + KH550) nanohybrids	714.29	[51]
$Cr(OH)_3$–NPs–CNC hybrid nanocomposite	106	[52]
Graphene nanosheet/magnetite composite	43.82	[53]
M-MWCNTs adsorbent	48.86	[54]
Poly(AA-co-AM)/MMT composites	1964.1	This work

MMT was subjected to desorption experiments using HCl solutions of different pH as eluent. As shown in Fig. 11a, the desorption rate of the adsorbent was the highest (85.1%) under strong acid (pH 2.0) conditions and decreased rapidly with the increase of eluent pH and reached a minimum value (0.23%) at pH 9.0. The results show that the MB molecule is immobilized on poly(AA-co-AM)/MMT by ion exchange or electrostatic attraction, and the effect of pH on adsorption is confirmed.

Reusability is an important indicator of the practical application of adsorbents. The effect of adsorption-desorption cycle on the adsorption performance of poly(AA-co-AM)/MMT is shown in Fig. 11b. After five adsorption-desorption cycles, the adsorbent adsorption capacity decreased slightly but still reached 96% of the initial capacity. The results show that poly(AA-co-AM)/MMT composites have good reusability and can effectively remove methylene blue in water after repeated treatment.

Comparison with other adsorbents

Poly(AA-co-AM)/MMT composites have a very high adsorption capacity for methylene blue compared to other reported montmorillonite, acrylic, or acrylamide-modified adsorbents. In addition, the preparation process of adsorbents such as HNTs/Fe_3O_4/poly(DA + KH550) nanohybrids and $Cr(OH)_3$–NPs–CNC hybrid nanocomposite are relatively complicated, while the adsorption activity of materials such as M-MWCNTs adsorbent and graphene nanosheet/magnetite composite is too low. Compared with the reported adsorbents (Table 4), poly(AA-co-AM)/MMT composites show very high adsorption activity, simple preparation process, and low preparation cost. Therefore, poly(AA-co-AM)/MMT composites can be used as efficient adsorbents for removing cationic dyes in wastewater.

Adsorption mechanism

The microstructure and surface groups of poly(AA-co-AM)/MMT, the structure of MB dyes, and the interaction between the binding sites and other factors all affect the adsorption properties of adsorbents. First, combined with FTIR, EDX, pH effects, and desorption studies, we propose three possible mechanisms for MB adsorption. The first is the electrostatic interaction between the –COO– of the adsorbent surface and the positively charged groups in the MB cationic dye. The second is that –COOH adsorbs MB cationic dyes directly through ion exchange. The third is the hydrogen bond interaction between O–H in the polymer and the positively charged groups in the MB cationic dye. Secondly, the influence of MMT content, XRD, and SEM shows that the introduction of small amounts of MMT can produce loose porous structures, so as to improve the adsorption capacity of the composites. Finally, the adsorption kinetics showed that the adsorption process was controlled by surface adsorption, intra-particle diffusion, and liquid-film diffusion mechanism. Adsorption isotherm studies show that MB is monolayer adsorbed on the adsorbent surface.

Conclusions

In this study, we successfully prepared a series of poly(AA-co-AM)/MMT composites by free radical polymerization and characterized by XRD, FTIR, SEM, and EDX. Batch adsorption experiments of MB show that the adsorption process of MB depends on MMT content, initial pH value, adsorption temperature, and ionic strength. The introduction of a small amount of MMT can produce a loose porous structure, which can improve the adsorption capacity of composite materials. The adsorption amount of MB on the composite increases with the increase of pH and is affected by the temperature change. The adsorption kinetic data are in good agreement with the pseudo-second-order kinetics model, and the adsorption process is controlled by the intra-particle diffusion and liquid-film diffusion mechanism. The adsorption equilibrium data agrees well with the Langmuir isothermal model, indicating that MB is monolayer adsorbed on the composite surface, and the theoretical maximum adsorption capacity is 1964.1 mg g^{-1}. Desorption studies show that the desorption rate of the composites was as high as 85.1%, and the adsorbent retains 96% of the initial adsorption capacity after five adsorption-desorption cycles. In addition, the study shows that the composite mainly adsorbs MB dye molecules through electrostatic attraction, ion exchange, and hydrogen bonding interaction. Therefore, poly(AA-co-AM)/MMT composites can be used as an economically efficient adsorbent for removing MB from wastewater.

Funding information We would like to thank the University of Fuzhou (School of Chemistry) for its financial and technical support.

Compliance with ethical standards

Conflict of interest The authors declare that they have no conflict of interest.

References

1. Liu F, Zou H, Hu J, Liu H, Peng J, Chen Y, Lu F, Huo Y (2016) Fast removal of methylene blue from aqueous solution using porous soy protein isolate based composite beads. Chem Eng J 287:410–418. https://doi.org/10.1016/j.cej.2015.11.041
2. Zhuang X, Wan Y, Feng C, Shen Y, Zhao D (2009) Highly efficient adsorption of bulky dye molecules in wastewater on ordered mesoporous carbons. Chem Mater 21(4):706–716. https://doi.org/10.1021/cm8028577
3. Rafatullah M, Sulaiman O, Hashim R, Ahmad A (2010) Adsorption of methylene blue on low-cost adsorbents: a review. J Hazard Mater 177(1–3):70–80. https://doi.org/10.1016/j.jhazmat.2009.12.047
4. Gong RM, Ding Y, Lie M, Yang C, Liu HJ, Sun YZ (2005) Utilization of powdered peanut hull as biosorbent for removal of anionic dyes from aqueous solution. Dyes Pigments 64(3):187–192. https://doi.org/10.1016/j.dyepig.2004.05.05
5. Ghosh D, Bhattacharyya KG (2002) Adsorption of methylene blue on kaolinite. Appl Clay Sci 20(6):295–300. https://doi.org/10.1016/s0169-1317(01)00081-3
6. Ma ZW, Kotaki M, Ramakrishna S (2005) Electrospun cellulose nanofiber as affinity membrane. J Membr Sci 265(1–2):115–123. https://doi.org/10.1016/j.memsci.2005.04.044
7. Verma AK, Dash RR, Bhunia P (2012) A review on chemical coagulation/flocculation technologies for removal of colour from textile wastewaters. J Environ Manag 93(1):154–168. https://doi.org/10.1016/j.jenvman.2011.09.012
8. Martinez-Huitle CA, Brillas E (2009) Decontamination of wastewaters containing synthetic organic dyes by electrochemical methods: a general review. Applied Catalysis B-Environmental 87(3–4):105–145. https://doi.org/10.1016/j.apcatb.2008.09.017
9. Hu E, Wu X, Shang S, Tao X-M, Jiang S-X, Gan L (2016) Catalytic ozonation of simulated textile dyeing wastewater using mesoporous carbon aerogel supported copper oxide catalyst. J Clean Prod 112:4710–4718. https://doi.org/10.1016/j.jclepro.2015.06.127
10. Saratale RG, Saratale GD, Chang JS, Govindwar SP (2011) Bacterial decolorization and degradation of azo dyes: a review. J Taiwan Inst Chem Eng 42(1):138–157. https://doi.org/10.1016/j.jtice.2010.06.006
11. Gupta VK, Kumar R, Nayak A, Saleh TA, Barakat MA (2013) Adsorptive removal of dyes from aqueous solution onto carbon nanotubes: a review. Adv Colloid Interf Sci 193:24–34. https://doi.org/10.1016/j.cis.2013.03.003
12. Alhashimi HA, Aktas CB (2017) Life cycle environmental and economic performance of biochar compared with activated carbon: a meta-analysis. Resources Conservation and Recycling 118:13–26. https://doi.org/10.1016/j.resconrec.2016.11.016
13. Crini G (2006) Non-conventional low-cost adsorbents for dye removal: a review. Bioresour Technol 97(9):1061–1085. https://doi.org/10.1016/j.biortech.2005.05.001
14. Hui B, Zhang Y, Ye L (2014) Preparation of PVA hydrogel beads and adsorption mechanism for advanced phosphate removal. Chem Eng J 235:207–214. https://doi.org/10.1016/j.cej.2013.09.045
15. Alvarez-Lorenzo C, Concheiro A (2002) Reversible adsorption by a pH- and temperature-sensitive acrylic hydrogel. J Control Release 80(1–3):247–257. https://doi.org/10.1016/s0168-3659(02)00032-9
16. Haraguchi K, Takehisa T (2002) Nanocomposite hydrogels: a unique organic-inorganic network structure with extraordinary mechanical, optical, and swelling/de-swelling properties. Adv Mater 14(16):1120–1124. https://doi.org/10.1002/1521-4095(20020816)14:16<1120::aid-adma1120>3.0.co;2-9
17. Choy J-H, Choi S-J, Oh J-M, Park T (2007) Clay minerals and layered double hydroxides for novel biological applications. Appl Clay Sci 36(1–3):122–132. https://doi.org/10.1016/j.clay.2006.07.007
18. Xue G, Gao M, Gu Z, Luo Z, Hu Z (2013) The removal of p-nitrophenol from aqueous solutions by adsorption using gemini surfactants modified montmorillonites. Chem Eng J 218:223–231. https://doi.org/10.1016/j.cej.2012.12.045
19. Zhu R, Chen Q, Zhou Q, Xi Y, Zhu J, He H (2016) Adsorbents based on montmorillonite for contaminant removal from water: a review. Appl Clay Sci 123:239–258. https://doi.org/10.1016/j.clay.2015.12.024
20. Chang J, Ma J, Ma Q, Zhang D, Qiao N, Hu M, Ma H (2016) Adsorption of methylene blue onto Fe3O4/activated montmorillonite nanocomposite. Appl Clay Sci 119:132–140. https://doi.org/10.1016/j.clay.2015.06.038
21. Shi Y, Xue Z, Wang X, Wang L, Wang A (2013) Removal of methylene blue from aqueous solution by sorption on lignocellulose-g-poly(acrylic acid)/montmorillonite three-dimensional cross-linked polymeric network hydrogels. Polym Bull 70(4):1163–1179. https://doi.org/10.1007/s00289-012-0898-4
22. Marrakchi F, Khanday WA, Asif M, Hameed BH (2016) Cross-linked chitosan/sepiolite composite for the adsorption of methylene blue and reactive orange 16. Int J Biol Macromol 93(Pt A):1231–1239. https://doi.org/10.1016/j.ijbiomac.2016.09.069
23. Shirsath SR, Patil AP, Bhanvase BA, Sonawane SH (2015) Ultrasonically prepared poly(acrylamide)-kaolin composite hydrogel for removal of crystal violet dye from wastewater. Journal of Environmental Chemical Engineering 3(2):1152–1162. https://doi.org/10.1016/j.jece.2015.04.016
24. Ayazi Z, Khoshhesab ZM, Azhar FF, Mohajeri Z (2017) Modeling and optimization of adsorption removal of reactive Orange 13 on the alginate-montmorillonite-polyaniline nanocomposite via response surface methodology. J Chin Chem Soc 64(6):627–639. https://doi.org/10.1002/jccs.201600876
25. Zhu L, Zhang L, Tang Y (2012) Synthesis of montmorillonite/poly(acrylic acid-co-2-acrylamido-2-methyl-1-propane sulfonic acid) superabsorbent composite and the study of its adsorption. Bull Korean Chem Soc 33(5):1669–1674. https://doi.org/10.5012/bkcs.2012.33.5.1669
26. Li S, Zhang H, Feng J, Xu R, Liu X (2011) Facile preparation of poly(acrylic acid-acrylamide) hydrogels by frontal polymerization and their use in removal of cationic dyes from aqueous solution. Desalination 280(1–3):95–102. https://doi.org/10.1016/j.desal.2011.06.056
27. Liu Y, Zheng Y, Wang A (2010) Enhanced adsorption of methylene blue from aqueous solution by chitosan-g-poly (acrylic acid)/vermiculite hydrogel composites. J Environ Sci 22(4):486–493. https://doi.org/10.1016/s1001-0742(09)60134-0
28. Andrini L, Moreira Toja R, Gauna MR, Conconi MS, Requejo FG, Rendtorff NM (2017) Extended and local structural characterization of a natural and 800 degrees C fired Na-montmorillonite-Patagonian bentonite by XRD and al/Si XANES. Appl Clay Sci 137:233–240. https://doi.org/10.1016/j.clay.2016.12.030
29. Morgan AB, Gilman JW (2003) Characterization of polymer-layered silicate (clay) nanocomposites by transmission electron microscopy and X-ray diffraction: a comparative study. J Appl Polym Sci 87(8):1329–1338. https://doi.org/10.1002/app.11884

30. Mansoori Y, Atghia SV, Zamanloo MR, Imanzadeh G, Sirousazar M (2010) Polymer-clay nanocomposites: free-radical grafting of polyacrylamide onto organophilic montmorillonite. Eur Polym J 46(9):1844–1853. https://doi.org/10.1016/j.eurpolymj.2010.07.006
31. Wang L, Zhang J, Wang A (2008) Removal of methylene blue from aqueous solution using chitosan-g-poly (acrylic acid)/montmorillonite superadsorbent nanocomposite. Colloids Surf A Physicochem Eng Asp 322(1–3):47–53. https://doi.org/10.1016/j.colsurfa.2008.02.019
32. Wang L, Zhang J, Wang A (2011) Fast removal of methylene blue from aqueous solution by adsorption onto chitosan-g-poly (acrylic acid)/attapulgite composite. Desalination 266(1–3):33–39. https://doi.org/10.1016/j.desal.2010.07.065
33. Inbaraj BS, Chiu CP, Ho GH, Yang J, Chen BH (2006) Removal of cationic dyes from aqueous solution using an anionic poly-gamma-glutamic acid-based adsorbent. J Hazard Mater 137(1):226–234. https://doi.org/10.1016/j.jhazmat.2006.01.057
34. Liu Y, Zheng Y, Wang A (2011) Effect of biotite content of hydrogels on enhanced removal of methylene blue from aqueous solution. Ionics 17(6):535–543. https://doi.org/10.1007/s11581-011-0552-4
35. Panic VV, Velickovic SJ (2014) Removal of model cationic dye by adsorption onto poly(methacrylic acid)/zeolite hydrogel composites: kinetics, equilibrium study and image analysis. Sep Purif Technol 122:384–394. https://doi.org/10.1016/j.seppur.2013.11.025
36. Mittal H, Maity A, Ray SS (2015) Gum ghatti and poly(acrylamide-co-acrylic acid) based biodegradable hydrogel-evaluation of the flocculation and adsorption properties. Polym Degrad Stab 120:42–52. https://doi.org/10.1016/j.polymdegradstab.2015.06.008
37. Hamdaoui O (2006) Batch study of liquid-phase adsorption of methylene blue using cedar sawdust and crushed brick. J Hazard Mater 135(1–3):264–273. https://doi.org/10.1016/j.jhazmat.2005.11.062
38. Zhou CJ, Wu QL, Lei TZ, Negulescu JI (2014) Adsorption kinetic and equilibrium studies for methylene blue dye by partially hydrolyzed polyacrylamide/cellulose nanocrystal nanocomposite hydrogels. Chem Eng J 251:17–24. https://doi.org/10.1016/j.cej.2014.04.034
39. Liu X, Wei Q (2016) Removal of methylene blue from aqueous solution using porous starch-g-poly(acrylic acid) superadsorbents. RSC Adv 6(83):79853–79858. https://doi.org/10.1039/c6ra14903k
40. Vaz MG, Pereira AGB, Fajardo AR, Azevedo ACN, Rodrigues FHA (2017) Methylene blue adsorption on chitosan-g-poly(acrylic acid)/rice husk ash superabsorbent composite: kinetics, equilibrium, and thermodynamics. Water Air Soil Pollut 228(1). https://doi.org/10.1007/s11270-016-3185-4
41. Wu FC, Tseng RL, Juang RS (2005) Comparisons of porous and adsorption properties of carbons activated by steam and KOH. J Colloid Interface Sci 283(1):49–56. https://doi.org/10.1016/j.jcis.2004.08.037
42. Horsfall Jr M, Vicente JL (2007) Kinetic study of liquid-phase adsorptive removal of heavy metal ions by almond tree (Terminalia catappa L.) leaves waste. Bull Chem Soc Ethiop 21(3):349–362
43. Lorenc-Grabowska E, Gryglewicz G (2007) Adsorption characteristics of Congo red on coal-based mesoporous activated carbon. Dyes Pigments 74(1):34–40. https://doi.org/10.1016/j.dyepig.2006.01.027
44. Oladipo AA, Gazi M, Saber-Samandari S (2014) Adsorption of anthraquinone dye onto eco-friendly semi-IPN biocomposite hydrogel: equilibrium isotherms, kinetic studies and optimization. J Taiwan Inst Chem Eng 45(2):653–664. https://doi.org/10.1016/j.jtice.2013.07.013
45. Daneshvar E, Kousha M, Jokar M, Koutahzadeh N, Guibal E (2012) Acidic dye biosorption onto marine brown macroalgae: isotherms, kinetic and thermodynamic studies. Chem Eng J 204:225–234. https://doi.org/10.1016/j.cej.2012.07.090
46. Salama A, Shukry N, El-Sakhawy M (2015) Carboxymethyl cellulose-g-poly(2-(dimethylamino) ethyl methacrylate) hydrogel as adsorbent for dye removal. Int J Biol Macromol 73:72–75. https://doi.org/10.1016/j.ijbiomac.2014.11.002
47. Li R, Liu L, Yang F (2014) Removal of aqueous Hg(II) and Cr(VI) using phytic acid doped polyaniline/cellulose acetate composite membrane. J Hazard Mater 280:20–30. https://doi.org/10.1016/j.jhazmat.2014.07.052
48. Mall ID, Srivastava VC, Kumar GVA, Mishra IM (2006) Characterization and utilization of mesoporous fertilizer plant waste carbon for adsorptive removal of dyes from aqueous solution. Colloids Surf A Physicochem Eng Asp 278(1–3):175–187. https://doi.org/10.1016/j.colsurfa.2005.12.017
49. Zhang J, Azam MS, Shi C, Huang J, Yan B, Liu Q, Zeng H (2015) Poly(acrylic acid) functionalized magnetic graphene oxide nanocomposite for removal of methylene blue. RSC Adv 5(41):32272–32282. https://doi.org/10.1039/c5ra01815c
50. Hamoud MA, Allan KF, Sanad WA, El-Hamouly SH, Ayoub RR (2014) Gamma irradiation induced preparation of poly(acrylamide-itaconic acid)/zirconium hydrous oxide for removal of Cs-134 radionuclide and methylene blue. J Radioanal Nucl Chem 302(1):169–178. https://doi.org/10.1007/s10967-014-3206-y
51. Wan XY, Zhan YQ, Long ZH, Zeng GY, He Y (2017) Core@double-shell structured magnetic halloysite nanotube nano-hybrid as efficient recyclable adsorbent for methylene blue removal. Chem Eng J 330:491–504. https://doi.org/10.1016/j.cej.2017.07.178
52. Nekouei F, Nekouei S, Keshtpour F, Noorizadeh H, Wang S (2017) Cr(OH)(3)-NPs-CNC hybrid nanocomposite: a sorbent for adsorptive removal of methylene blue and malachite green from solutions. Environ Sci Pollut Res 24(32):25291–25308. https://doi.org/10.1007/s11356-017-0111-2
53. Ai L, Zhang C, Chen Z (2011) Removal of methylene blue from aqueous solution by a solvothermal-synthesized graphene/magnetite composite. J Hazard Mater 192(3):1515–1524. https://doi.org/10.1016/j.jhazmat.2011.06.068
54. Ai L, Zhang C, Liao F, Wang Y, Li M, Meng L, Jiang J (2011) Removal of methylene blue from aqueous solution with magnetite loaded multi-wall carbon nanotube: kinetic, isotherm and mechanism analysis. J Hazard Mater 198:282–290. https://doi.org/10.1016/j.jhazmat.2011.10.041